DOI: 10.1002/ejic.200900607

Tartatric Acid and L-Cysteine Synergistic-Assisted Synthesis of Antimony Trisulfide Hierarchical Structures in Aqueous Solution

Jun Pan,[a] Shenglin Xiong,[a] Baojuan Xi,[a] Jiangfa Li,[a] Jiangying Li,[a] Hongyang Zhou,[a] and Yitai Qian*[a]

Keywords: Hierarchical structures / Hydrothermal synthesis / Antimony / Amino acids / Chalcogens

Alveolate amorphous Sb_2S_3 microspheres about 2 μm in diameter were hydrothermally synthesized in aqueous solution without the use of a surfactant at 180 °C by using $SbCl_3$, L-cysteine, and tartaric acid as starting materials. After annealing at 250 °C for 3 h under a nitrogen atmosphere, polycrystalline Sb_2S_3 hollow spheres were obtained. The morphology, structure, and phase composition of alveolate Sb_2S_3 microspheres were characterized by X-ray diffraction, field-emission scanning electron microscopy, energy dispersive X-ray analysis, and X-ray photoelectron spectroscopy. It was demonstrated that tartaric acid and L-cysteine play a key role in the formation of such hierarchical structures. In addition, the possible aggregation mechanism was proposed to illustrate the formation of Sb_2S_3 microspheres on the basis of the experimental results and analyses.

(© Wiley-VCH Verlag GmbH & Co. KGaA, 69451 Weinheim, Germany, 2009)

Introduction

As an important V-VI group binary chalcogenide, antimony sulfide (Sb_2S_3) with an energy band gap varying between 1.5 and 2.2 eV has attracted particular attention owing to its good photovoltaic properties and high thermoelectric power,[1] and it has been applied in various areas of television cameras with photoconducting targets, thermoelectric devices, electronic and optoelectronic devices, and in infrared (IR) spectroscopy.[2] So far, various morphologies and architectures of Sb_2S_3 nanostructures have been reported, such as microtubes,[3] hollow cones,[4] whiskers,[5] dendritic-like, featherlike microstructures,[6] hollow olivary architectures,[7] nanorod-bundles,[8] and sheaf-like hierarchical nanostructure.[9] Besides the above shapes, Sb_2S_3 microspheres also have been intensively studied and many efforts have been devoted to their fabrication. Cheng et al.[10] prepared Sb_2S_3 microspheres by a one-step, ambient-temperature reaction in ethanol solution. Hu et al.[11] used $SbCl_3$ and $NH_2NHCSNH_2$ at 140 °C in ethanol solution to gain prism-sphere-like and prickly sphere-like Sb_2S_3. Hollow Sb_2S_3 microspheres[12] were realized by the groups of Shen and Cao through a chemical conversion method and a convenient Ostwald ripening route, respectively. However, in this article, Sb_2S_3 microspheres with an alveolate superstructure, which is a structure that has not been reported previously, have been synthesized by the present route.

In regard to the preparation of various nanostructures, a biomaterial-based templating technique for the synthesis and assembly of artificial structures of crystalline inorganic materials has displayed promise.[13] In the growth process of nanostructures, these biomaterials serve as capping ligands and bind on some facets, which always lead to various novel shapes. Among these biomolecules, L-cysteine, a very important member with three functional groups (-SH, -NH_2, -COOH), has strong coordinating ability with inorganic cations. It has thus been exploited to form different architectures, such as quantum dots,[14] nanotubes,[15] dendritic structures,[16] 3D spherical nanostructures from nanorods,[17] and flower-like patterns with nanorods.[18]

Herein, we report the hydrothermal synthesis of Sb_2S_3 microspheres with alveolate superstructures by using $SbCl_3$ and L-cysteine as raw materials without any surfactants. The time-dependent experiments were performed to explore temporal morphological evolution, and a growth mechanism was proposed to illustrate the formation process.

Results and Discussion

The phase and purity of the as-obtained products were characterized by XRD analysis. Figure 1a is the XRD pattern of the sample prepared at 180 °C, which shows the sample was amorphous. When annealed at 250 °C for 3 h, obvious diffraction peaks of the sample appeared, as shown in Figure 1b. All of the clear diffraction peaks can be inde-

[a] Department of Chemistry, Hefei National Laboratory for Physical Sciences at Microscale and Department of Materials Science & Engineering, University of Science and Technology of China,
Hefei, Anhui 230026, China
Fax: +86-551-3607234
E-mail: ytqian@ustc.edu.cn

Supporting information for this article is available on the WWW under http://dx.doi.org/10.1002/ejic.200900607.

 WILEY InterScience DISCOVER SOMETHING GREAT © 2009 Wiley-VCH Verlag GmbH & Co. KGaA, Weinheim

xed to orthorhombic Sb_2S_3 with lattice parameters a = 11.22 Å, b = 11.31 Å, c = 3.839 Å (JCPDS 06-0474). No peaks attributable to Sb_2O_3 or other impurities were observed.

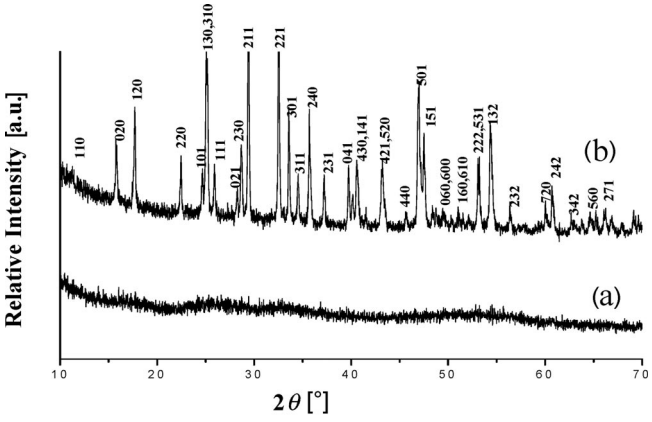

Figure 1. XRD pattern of the as-obtained Sb_2S_3 microspheres: (a) obtained at 180 °C under hydrothermal condition, (b) annealed at 250 °C for 3 h.

Figure 2 is the SEM image of Sb_2S_3 microspheres fabricated at 180 °C for 12 h, clearly showing that these spheres with a saccate surface are about 2 μm in diameter. Remarkably, some broken spheres in the SEM image reveal their interior structures consisting of alveolate particles presented in Figure 2b. The SEM image of sample annealed at 250 °C for 3 h is shown in Figure 2c, from which the slippery sphere with a hollow structure was formed (Figure 2d). An energy dispersive X-ray analysis (EDX) technique was used to characterize the sample obtained at 180 °C. The detected peaks in the EDX spectrum, shown in Figure 2e, are assigned to S and Sb. A single peak at 2.3 keV is assigned to S K_α, whereas a group of four peaks located in the region of higher energy is assigned to Sb L_α. The EDX spectrum was recorded from large sample areas, consequently representing an average elemental composition of antimony trisulfide. At the same time, the result demonstrates that the molar ratio of Sb/S obtained from the peak areas is 38.52:61.48, which is close to 2:3. The Sb 3d orbital peaks (529.2, 538.3 eV) in the X-ray photoelectron spectroscopy (XPS) spectrum confirms that the oxidation state of antimony is Sb^{III}[19] (Figure 2f).

The complexing agent (tartaric acid) exerts an important influence on the growth of the Sb_2S_3 microspheres. When the concentration of tartaric acid was low (2 mmol), irregular Sb_2S_3 microspheres with flabby structures were gained (Figure 3a). If the concentration was high (10 mmol), approximately similar Sb_2S_3 microspheres were obtained and amorphous Sb_2S_3 with another typical wire-bundle morphology coexisted (Figure 3b). The high-magnification images of the wire bundle are shown in Figure 3c,d. However, when the experiment was carried out in the absence of tartaric acid with other conditions unchanged, $SbCl_3$ strongly hydrolyzed to produce a white precipitate, [$Sb(OH)_2$-

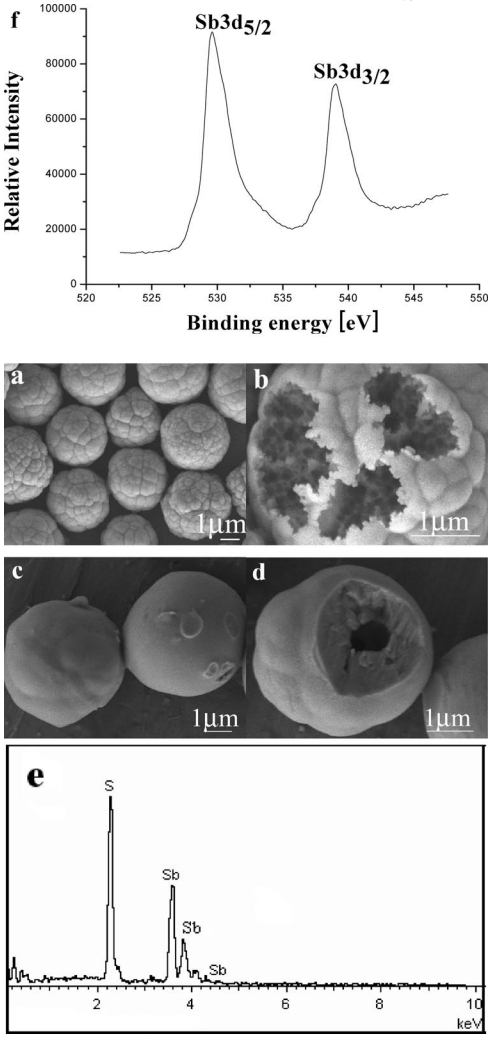

Figure 2. (a) SEM image of Sb_2S_3 microspheres prepared at 180 °C for 12 h; (b) SEM image of a single broken microsphere; (c) SEM image of Sb_2S_3 microspheres after annealing at 250 °C for 3 h; (d) SEM image of a single annealed sample; (e) EDX spectrum and (f) XPS spectrum of Sb 3d orbital peaks of antimony sulfide microspheres obtained at 180 °C after 12 h.

Cl], and not microspheres but irregular rod-like Sb_2S_3 was observed (see Supporting Information). As described above, the product obtained with 6 mmol of tartaric acid produced a regular microsphere 2 μm in diameter. On the basis of the results, the different concentration of the complexing agent might be the cause for these phenomena. However, the reaction is optimized for 6 mmol of the complexing agent, leading to the formation of regular microspheres as the final product. When the same reaction was carried out in an autoclave at 120 or 220 °C for 12 h, amorphous Sb_2S_3 was obtained with minor differences in morphology (Figure 3e,f).

L-Cysteine plays a crucial role in the growth of the Sb_2S_3 microspheres. Without changing other conditions, several different sulfurization reagents were used, such as, CS_2, CH_3CSNH_2, and CSN_2H_4. However, nonsphere-like structures were obtained when using these sulfurization reagents.

 © 2009 Wiley-VCH Verlag GmbH & Co. KGaA, Weinheim

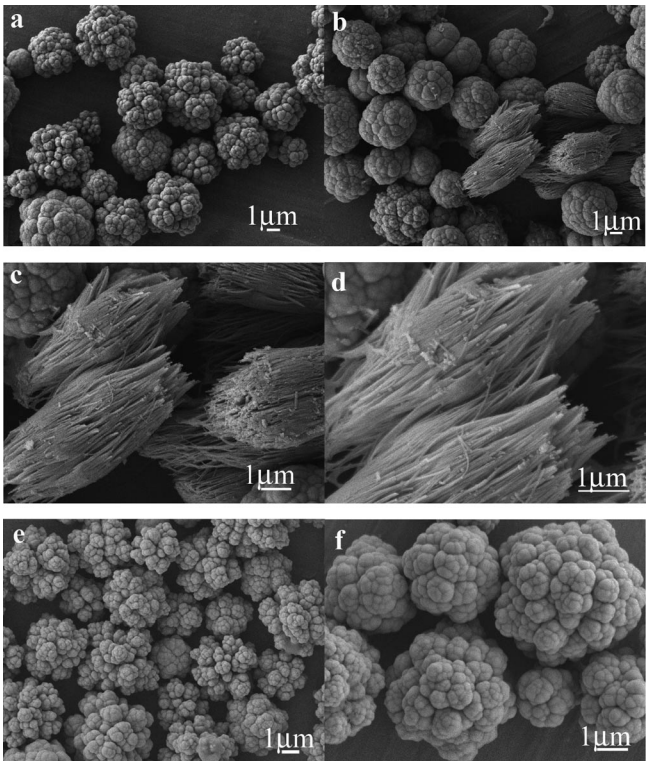

Figure 3. SEM images of the as-synthesized Sb_2S_3 with different concentrations of the complexing agent: (a) 2 mmol and (b) 10 mmol; (c) and (d) SEM images with different magnification of the typical wire-bundle structures; (e) and (f) SEM images of the as-synthesized Sb_2S_3 at 120 and 220 °C after 12 h, respectively.

Irregular brick-like Sb_2S_3 structures were gained when using CS_2 as reagents (Figure 4a). Rod-bundle-like Sb_2S_3 were synthesized by using CH_3CSNH_2 as the starting material (Figure 4b). Similarly, irregular rod-like Sb_2S_3 crystals were formed when using CSN_2H_4 as a reagent (Figure 4c). XRD results of the samples obtained by using different sulfurization reagents are shown in the Supporting Information. On the basis of the above results, we proposed that the reaction system containing L-cysteine and tartatric acid play a crucial role in the synthesis of the amorphous phase of Sb_2S_3. First, the Sb^{III} ion cooperated with the tartatric acid molecule. Then, L-cysteine coupled tightly with the tartatric acid molecule to form a compact net-like structure owing to hydrogen-bonding effects. With an increase in temperature, the tartatric acid molecule and L-cysteine degraded and Sb_2S_3 was formed but with isotropic properties. So the final products are amorphous phase.

A series of time-dependent experiments were conducted to track the formation process of the alveolate structures of Sb_2S_3. As shown in Figure 3, when the reaction time was 0.5 h, amorphous brick-like products composed of myriad nanoparticles were observed (Figure 5a). If the reaction lasted for another 15 min, sphere-like particles were predominantly obtained (Figure 5b). After 1 h of reaction, large numbers of Sb_2S_3 microspheres with a saccate surface were produced (Figure 5c). Uniform Sb_2S_3 large microspheres with diameters of about 2.5 μm were assembled from several smaller microspheres, which is consistent with the products obtained after 2 h (Figure 5d). When the reaction time was prolonged to 6 h, some of the large microspheres were compressed into compact structures (Figure 5e). Interestingly, when the reaction was terminated after 12 h, uniform microspheres with a smooth surface were formed (Figure 5f). As a result, the formation equation at our processing temperature may be formulated as follows:

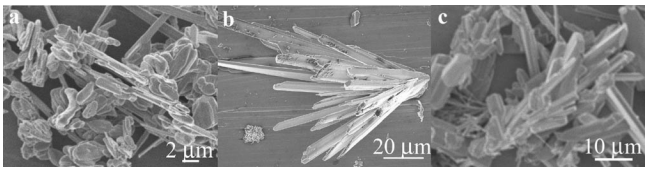

Figure 4. SEM images of the as-synthesized Sb_2S_3 by using different sources of sulfur while keeping other conditions unchanged: (a) CS_2, (b) CH_3CSNH_2, and (c) CSN_2H_4.

$$Sb^{III} + tart \rightarrow Sb^{III}(tart)$$

$$HSCH_2CH(NH_2)COOH \rightarrow -CH_2CH(NH_2)COO^- + 2H^+ + S^{2-}$$

$$2Sb^{III}(tart) + 3S^{2-} \rightarrow Sb_2S_3\downarrow + 2tart.$$

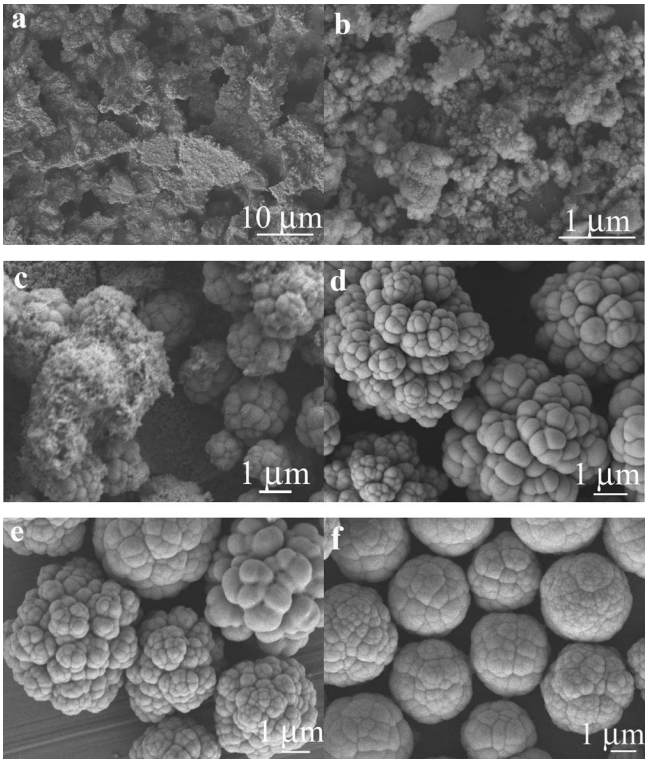

Figure 5. SEM images of the as-synthesized Sb_2S_3 with different reaction times: (a) 30 min, (b) 45 min, (c) 1 h, (d) 2 h, (e) 6 h, and (f) 12 h.

On the basis of the above discussion, the possible aggregation mechanism for the formation of the alveolate Sb_2S_3 microspheres is illustrated in Figure 6. Sb_2S_3 irregular nanoparticle aggregates are formed at the early stages of the reaction and then agglomerate into near-spherical particles,

 © 2009 Wiley-VCH Verlag GmbH & Co. KGaA, Weinheim

which subsequently grow together into sphere-like structures about 2 μm in diameter to minimize the system surface energy. With increasing reaction time, these primitive blocking units of nanoparticles aggregate into near-sphere-like substances then self-assemble into larger spheriform structures. The big spheriform structures are compressed to form a compact morphology driven by the tendency to reduce their surface energy.

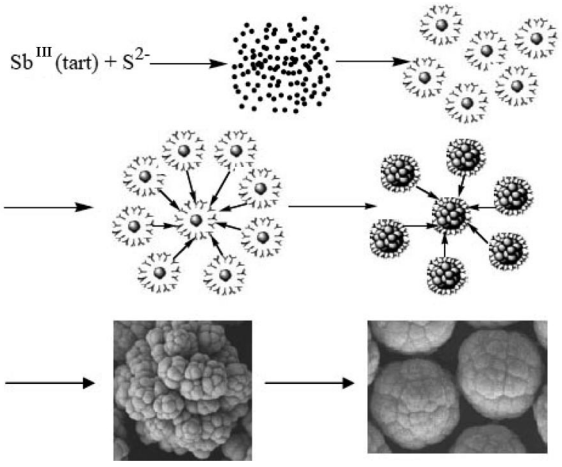

Figure 6. A schematic illustration for the formation of alveolate Sb_2S_3 microspheres.

Conclusions

In summary, alveolate Sb_2S_3 microspheres were successfully prepared through a simple hydrothermal method by using $SbCl_3$, L-cysteine, and tartaric acid as raw materials without the use of any surfactants in aqueous solution. The morphological evolution of the alveolate Sb_2S_3 microspheres was studied through time-dependent experiments. The complexing agent and L-cysteine acted as important parameters for the formation of sphere-like hierarchical structures. On the basis of the results, the formation process of the microspheres was proposed. The synthesized Sb_2S_3 microspheres may be useful in optoelectronic switches or photocatalysts.

Experimental Section

Sb_2S_3 Preparation: All of the chemicals were of analytical grade and used as received. In a typical experiment, tartaric acid (6 mmol) was dissolved in pure distilled water (45 mL) in a beaker, and antimony trichloride ($SbCl_3$; 1 mmol) was added into the above solution whilst stirring at room temperature. The solution was stirred strongly for about 30 min until it became clear. After that, L-cysteine (1.5 mmol) was added to the beaker, and the mixture was stirred for another 10 min. Then, the clear mixture was transferred into a Teflon-lined stainless-steel autoclave with a capacity of 60 mL. The autoclave was sealed and maintained at 180 °C for 12 h and then cooled to room temperature naturally. The precipitate was collected and washed with distilled water and absolute ethanol (3×), respectively. Then, the samples were dried in a vacuum at 50 °C for 6 h.

Characterization: The products were characterized by X-ray diffraction (XRD) recorded with a Japanese Rigaku D/max-γA rotating anode X-ray diffractometer equipped with monochromatic high-intensity Cu-K_α radiation (λ = 1.54178 Å). SEM images were taken with a field emission scanning electron microscope (FESEM, JEOL-6300F, 15 kV). X-ray photoelectron spectroscopy (XPS) measurements were performed with a VGESCALAB MKII X-ray photoelectron spectrometer with a Mg-K_α excitation source (1253.6 eV).

Supporting Information (see footnote on the first page of this article): SEM image and XRD pattern of the as-synthesized Sb_2S_3 without complexing agent at 180 °C along with XRD patterns of the as-synthesized Sb_2S_3 by using different sources of sulfur.

Acknowledgments

We greatly acknowledge financial support from 973 Project of China (Grant No. 2005CB623601) and the China Postdoctoral Science Foundation (No. 200801236).

[1] a) S. Ibuke, S. Yochimatsu, *J. Phys. Soc. Jpn.* **1955**, *10*, 549; b) B. Roy, B. R. Chakbraborty, R. Bhattacharya, A. K. Dutta, *Solid State Commun.* **1978**, *25*, 937; c) M. T. S. Nair, Y. Pena, J. Campos, V. M. Garcia, P. K. Nair, *J. Electrochem. Soc.* **1998**, *145*, 2113.
[2] a) N. Kh. Abrikosov, V. F. Bankina, L. V. Poretakaya, L. E. Shelimova, E. V. Skudnova in *Semiconducting II–VI and V–VI Compounds* (Ed.: A. Tybulewicz), Plenum, New York, **1969**, p. 186; b) D. Arivuoli, F. D. Gnanam, P. Ramasamy, *J. Mater. Sci. Lett.* **1988**, *7*, 711.
[3] X. W. Zheng, Y. Xie, L. Y. Zhu, X. C. Jiang, Y. B. Jia, W. H. Song, Y. P. Sun, *Inorg. Chem.* **2002**, *41*, 455–461.
[4] X. B. Cao, L. Gu, W. C. Wang, W. J. Gao, L. J. Zhuge, Y. H. Li, *J. Cryst. Growth* **2006**, *286*, 96–101.
[5] a) H. Wang, J. J. Zhu, H. Y. Chen, *Chem. Lett.* **2002**, *12*, 1242–1243; b) H. Wang, J. M. Zhu, J. J. Zhu, L. M. Yuan, H. Y. Chen, *Langmuir* **2003**, *19*, 10993–10996.
[6] H. M. Hu, Z. P. Liu, B. J. Yang, M. S. Mo, Q. W. Li, W. C. Yu, Y. T. Qian, *J. Cryst. Growth* **2004**, *262*, 375–382.
[7] Q. F. Han, J. Lu, X. J. Yang, L. D. Lu, X. Wang, *Cryst. Growth Des.* **2008**, *8*, 395–398.
[8] Q. F. Lu, H. B. Zeng, Z. Y. Wang, X. L. Cao, L. D. Zhang, *Nanotechnology* **2006**, *17*, 2098–2104.
[9] G. Y. Chen, B. Dneg, G. B. Cai, T. K. Zhang, W. F. Dong, W. X. Zhang, A. W. Xu, *J. Phys. Chem. C* **2008**, *112*, 672–679.
[10] B. Cheng, E. T. Samulski, *Mater. Resear. Bull.* **2003**, *38*, 297–301.
[11] H. M. Hu, Z. P. Liu, B. J. Yang, M. S. Mo, Q. W. Li, W. C. Yu, Y. T. Qian, *J. Cryst. Growth* **2004**, *262*, 375–382.
[12] a) X. B. Cao, L. Gu, L. J. Zhuge, W. J. Gao, W. C. Wang, S. F. Wu, *Adv. Funct. Mater.* **2006**, *16*, 896–902; b) Y. F. Zhu, D. H. Fan, W. Z. Shen, *Langmuir* **2008**, *24*, 11131–11136.
[13] a) J. Aizenberg, D. A. Muller, J. L. Grazul, D. R. Hamann, *Science* **2003**, *299*, 1205–1208; b) C. B. Mao, D. J. Solis, B. D. Reiss, S. T. Kottmann, R. Y. Sweeney, A. Hayhurst, G. Georgiou, B. Iverson, A. M. Belcher, *Science* **2004**, *303*, 213–217; c) H. J. Liang, T. E. Angelini, P. V. Braun, G. C. L. Wong, *J. Am. Chem. Soc.* **2004**, *126*, 14157–14165; d) J. L. Zhang, J. M. Du, B. X. Han, Z. M. Liu, T. Jiang, Z. F. Zhang, *Angew. Chem.* **2006**, *118*, 1134–1137; *Angew. Chem. Int. Ed.* **2006**, *45*, 1116–1119.
[14] J. H. Gao, G. L. Liang, B. Zhang, Y. Kuang, X. X. Zhang, B. Xu, *J. Am. Chem. Soc.* **2007**, *129*, 1428–1433.

 © 2009 Wiley-VCH Verlag GmbH & Co. KGaA, Weinheim

[15] H. Tong, Y. J. Zhu, L. X. Yang, L. Li, L. Zhang, *Angew. Chem.* **2006**, *118*, 7903–7906; *Angew. Chem. Int. Ed.* **2006**, *45*, 7739–7742.
[16] J. H. Xiang, H. Q. Cao, Q. Z. Wu, S. C. Zhang, X. R. Zhang, *Cryst. Growth Des.* **2008**, *8*, 3935–3940.
[17] S. L. Xiong, B. J. Xi, C. M. Wang, G. F. Zou, L. F. Fei, W. Z. Wang, Y. T. Qian, *Chem. Eur. J.* **2007**, *13*, 3076–3081.
[18] B. Zhang, X. C. Ye, W. Y. Hou, Y. Zhao, Y. Xie, *J. Phys. Chem. B* **2006**, *110*, 8978–8985.
[19] R. P. Vasquez, F. J. Grunthaner, *J. Appl. Phys.* **1981**, *52*, 3509–3514.

Received: June 30, 2009
Published Online: November 11, 2009

 © 2009 Wiley-VCH Verlag GmbH & Co. KGaA, Weinheim